Applied Catalysis B: Environmental 164 (2015) 352–359

Contents lists available at ScienceDirect

Applied Catalysis B: Environmental

journal homepage: www.elsevier.com/locate/apcatb

Preparation of homogeneous nitrogen-doped mesoporous TiO_2 spheres with enhanced visible-light photocatalysis

Xiao Li [a], Pengwei Liu [a], Yu Mao [a], Mingyang Xing [a,*], Jinlong Zhang [a,b,*]

[a] Key Lab for Advanced Materials and Institute of Fine Chemicals, East China University of Science and Technology, Shanghai 200237, PR China
[b] Department of Chemistry, Tsinghua University, Beijing 100084, PR China

ARTICLE INFO

Article history:
Received 8 August 2014
Received in revised form
13 September 2014
Accepted 19 September 2014
Available online 28 September 2014

Keywords:
Titanium dioxide sphere
Homogeneous
Nitrogen-doped
Mesoporous
Photocatalysis

ABSTRACT

A series of mesoporous TiO_2 spheres of nanosized crystals with high monodispersity and dimensional homogeneity are synthesized by a simple reflux method. In order to improve the visible light response and to further narrow the band bap of TiO_2 sphere, nitrogen is used as the dopant in a hydrothermal method. Different from the traditional nitrogen doping in TiO_2 solid sphere, the nitrogen is uniformly distributed from bulk to the surface of mesoporous TiO_2 sphere, which is beneficial to the generation of the successive energy bands inside the TiO_2 band gap. Interestingly, the XPS results indicate that the nitrogen doping concentration could reach 1.31% (only 0.17% for nitrogen doped solid TiO_2 sphere), owing to the homogeneous doping in the mesoporous TiO_2 spheres. The nitrogen doped TiO_2 spheres exhibit such excellent characteristics as high specific area, relatively small particle size, pure anatase phase and excellent UV–vis absorption capacity in the range of 400–800 nm, which are all beneficial to the photodegradation of Rhodamine B under the visible light irradiation. The high photocatalytic activity could be ascribed to the homogeneous nitrogen doping on the deep adjustment of energy band of TiO_2 sphere from the bulk to the surface.

1. Introduction

Titanium dioxide (TiO_2) has been known as one of the most promising photocatalytic materials and attracted much attention due to its good stability, nontoxicity, high efficiency and low cost [1–3]. However, TiO_2 with the wide band gap (E_g = 3.2 eV) can only absorb the near-UV light (λ < 380 nm)[4], which greatly limits its practical applications. In order to overcome this shortcoming, the appropriate modifications such as non-metal doping and metal doping are essential for TiO_2 to make maximum use of the visible-light region of sun. In the past few years, plenty of researches have been reported that doping TiO_2 with non-metal elements, such as carbon, boron, fluorine and nitrogen demonstrated enhanced visible light photocatalytic activities [5–8]. Among them, nitrogen doping has been proved to be a simple and effective method to attain visible-light photocatalysis [9]. However, most of studies on nitrogen doped TiO_2 considered that the nitrogen doping is only a surface or sub-surface modification and difficult to narrow the band gap in the bulk of TiO_2, thus, it could only improve the visible light absorption in the range of 400–600 nm. It is really difficult to achieve the absorption in the wider region of 400–800 nm only by the heterogeneous nitrogen doping.

In addition to focus on the improvement of visible light absorption, more and more researchers paid attention to the modification of microstructure of TiO_2, such as the TiO_2 with mesoporous structure. Both high specific surface area and porous frameworks are important characteristics of mesoporous TiO_2, which may exhibit large pore volume or large pore diameter [10] and are beneficial to such applications as photocatalytic activity or electrochemical activity. For example, Hao et al. [11] prepared mesoporous titania powders with a bicrystalline (anatase and brookite) framework by a modified sol–gel method. The as-prepared sample showed high photocatalytic activity to degrade Rhodamine B (RhB), which was attributed to the porous structure and large surface area. In addition, Zhou et al. [12] synthesized anatase TiO_2 with mesoporous structure by a unique hydrothermal process, applied in Lithium-based storage devices as an electrode material. Due to its large active surface area, the sample would allow for the use of high electrochemical reaction rates and is of great importance in battery applications.

Therefore, we can make out that the formation of mesoporous structure could improve the performance of TiO_2. Beyond that, the changing of morphology of TiO_2 is also an effective means to

* Corresponding authors at: Key Laboratory for Advanced Materials and Institute of Fine Chemicals, East China University of Science and Technology, Shanghai 200237, PR China. Tel.: +86 21 64252062; fax: +86 21 64252062.
E-mail addresses: mingyangxing@ecust.edu.cn (M. Xing), jlzhang@ecust.edu.cn (J. Zhang).

http://dx.doi.org/10.1016/j.apcatb.2014.09.053
0926-3373/

adjust the characteristics of TiO_2 [13,14]. There are various TiO_2 nanostructures reported, like nanotubes [15], nanoparticles (NPs) [16], nanowires [17], nanosheets [18] and so on. Particularly, three-dimensional (3D) TiO_2 sphere has attracted great interest because of its wide applications in photocatalysis and energy conversion [19,20]. However, the general TiO_2 powder or TiO_2 sphere still faces such difficulties as aggregation, uncontrolled size and low uniformity and so on. For example, Grosso et al. [21] adopted a one-step method combined with sol–gel chemistry to prepare nanocrystalline transition metal oxide spheres with controlled multi-scale porosity. It can be observed from TEM images that the TiO_2 spheres have poor dispersibility and the sizes are messy, which greatly limit their wide applications. The irregular morphology and lower surface area of powder TiO_2 always lead to the heterogeneous and low doping concentration of impurities in the bulk of TiO_2.

Apart from the physical improvements, hitherto, some researches about mesoporous TiO_2 spheres with nitrogen doping have been reported. Wu et al. [22] prepared visible-light-responsive nitrogen doped TiO_2 hollow spheres by acid-catalyzed hydrolysis using carbon spheres as a hard template and urea as a nitrogen source. Jung et al.[23] synthesized spherical pure anatase TiO_2 spheres with a mesoporous structure and high surface area of 116.5 m^2/g by a simple urea-assisted hydrothermal process. The sample was applied as dye-sensitized solar-cell electrodes and achieved 7.54% of conversion efficiency. However, the nanoparticles prepared above tended to be huddled together and presented irregular shapes, so the nitrogen sources are really difficult to enter into the bulk of TiO_2 spheres. Thus in order to improve the photocatalytic activity of TiO_2, these issues should be addressed wisely and need an appropriate strategy.

Above all, it will be of great significance to have perfect control over the physical or chemical properties if the morphology and chemical composition of the porous material with a nanometre scale could be manipulated well. Therefore, in this work, a series of mesoporous TiO_2 spheres with high monodispersity and dimensional homogeneity are synthesized. Owing to the unique spherical structure consisted of nanocrystals, uniform pore size distribution and high surface area, further nitrogen doping modification can achieve a homogeneous doping and produce uniform and high concentration of nitrogen, which is expected to narrow the band gap of TiO_2 sphere from bulk to surface and enhance the photocatalytic activity of TiO_2 under the visible light irradiation for the degradation of RhB.

2. Experimental

2.1. Preparation of mesoporous titanium dioxide spheres

Mesoporous TiO_2 spheres were synthesized via a modified sol–gel method with polyvinylpyrrolidone (PVP) as dispersant and $Ti(SO_4)_2$ as Ti precursor. Besides, dodecyltrimethylammonium bromide (CTAB) was added as a sort of soft template or pore-forming agent. In a typical process, 2 g of $Ti(SO_4)_2$ or 2 g of PVP with 0.4 g of CTAB was dissolved into a mixture of certain amount of n-propanol and deionized water, respectively. The obtained two solutions were blended together and stirred for 15 min at room temperature. Subsequently, the transparent mixture was heated to 70 °C and kept for another 2 h. After it cooled to the ambient temperature naturally, the precipitates were collected through vacuum filtering, and washed for several times with deionized water and ethanol, then dried overnight at 80 °C. Up to this step, the obtained sample was marked as TiO_2 precursor. Finally, the precursor was calcined at 400 °C for 2 h with a heating rate of 1 °C/min to be mesoporous TiO_2 spheres, denoted as m-TiO_2.

By contrast, the pure TiO_2 solid sphere as control sample was achieved in the absence of CTAB and denoted as p-TiO_2.

2.2. Preparation of nitrogen doped mesoporous titanium dioxide spheres

To prepare nitrogen doped mesoporous TiO_2 spheres, ammonia was adopted as the nitrogen source in a hydrothermal process. The detailed procedure was as follows: 0.2 g of TiO_2 precursor was added into a mixture of 8 mL deionized water and 12 mL of ethanol in a cylindrical vessel. Then a certain amount of ammonia was put into the suspension under stirring and the mixture was stirred for 2 h to get a uniform solution. Subsequently, the mixed solution was transferred into a 50 mL Teflon-lined autoclave and kept at 180 °C for 12 h. The product was centrifugated, washed and dried at 80 °C. The final sample was obtained via calcination at 400 °C for 2 h with a 1 °C/min heating rate. The sample of nitrogen doped mesoporous TiO_2 sphere was marked as n-N-TiO_2 where n represents the mole ratio of ammonia to TiO_2, chosen as 2, 1, 0.8, 0.5, 0.2, 0.

By contrast, the solid p-TiO_2 sphere was treated by a same method to prepare the nitrogen doped solid TiO_2 sphere, which was denoted as N-p-TiO_2.

2.3. Characterization

The morphologies were characterized by transmission electron microscopy (TEM, JEM2000EX) and scanning electron microscopy (SEM, JEOL JSM-6360 LV). X-ray diffraction (XRD) measurements were carried with Rigaku Ultima IV (Cu Kα radiation, λ = 1.5406 Å) in the range of 10–80° (2θ). The instrument, a Perkin-Elmer PHI 5000C ESCA system with Al Kα radiation, was adopted to acquire the data of X-ray photoelectron spectroscopy (XPS). The shift of the binding energy was referred to the C1s level at 284.6 eV as an internal standard. The room-temperature Raman analysis of samples was performed using a inVia Reflex Raman spectrometer with 524.5 nm laser excitation. The X-band electron paramagnetic resonance (EPR) spectra of samples were collected at liquid nitrogen temperature using Bruker EMX-8/2.7 spectrometer. The Brunauer–Emmett–Teller (BET) surface areas of the prepared samples were obtained from N_2 adsorption–desorption isotherms at liquid nitrogen temperature using a Micromeritics ASAP 2020 system. UV–vis absorption spectra were obtained using a scan UV–vis spectrophotometer (Varian Cary 500) equipped with an integrating sphere assembly, while $BaSO_4$ was used as reference.

2.4. Measurement of photocatalytic activity

The photocatalytic activity was evaluated by analyzing the degradation of Rhodamine B (RhB) (10 mg/L) under visible light irradiation. And a 1000 W tungsten halogen lamp equipped with a UV cut-off filter (λ > 420 nm) was used as a visible light source in the home made photo-reactor, having a wooden box fitted with a quartz jacket containing a water circulation facility to maintain the temperature below 40 °C. 50 mg of as-prepared sample was added into 50 mL of RhB solution in a 100 mL quartz tube and carried out ultrasonic for 1 min. Subsequently, the suspension was stirred in the dark for 1 h to obtain the adsorption–desorption equilibrium on the surface of the catalyst. At given time intervals, about 5 mL of the dispersion was sampled and centrifuged. The filtrates were analyzed by recording variations in the absorption in UV–vis spectra of RhB, using a UV–vis spectrophotometer.

3. Results and discussion

The formation process of nitrogen doped mesoporous TiO_2 spheres can be explained through the schematic illustration shown

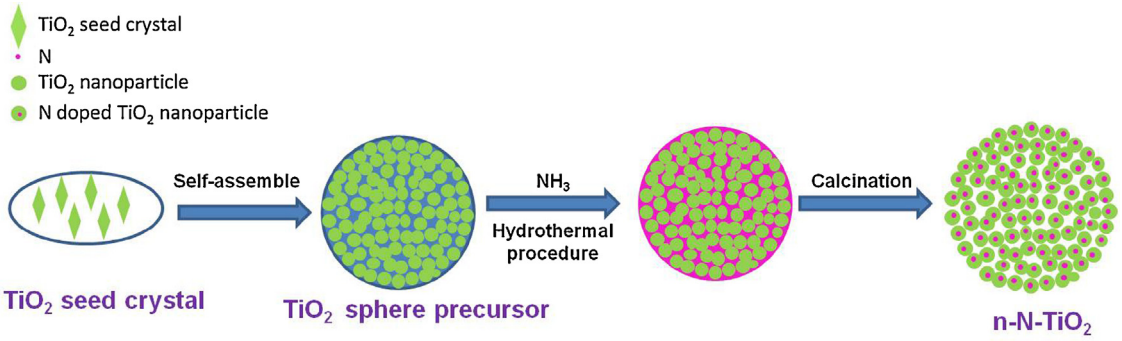

Scheme 1. Schematic diagram of the formation process of nitrogen doped mesoporous TiO_2 spheres.

in Scheme 1. Firstly, TiO_2 seed crystals grow into TiO_2 nanoparticles in size of 12 nm, and then self-assemble together into TiO_2 sphere precursor in the presence of PVP and CTAB. The PVP can not only increase the Zeta potential of inter-particles repulsion, but also form a steric hindrance, which can reduce the contact between different reactive molecules and decrease the reaction rate. The decrease of nucleation and growth rate is beneficial for the formation of TiO_2 sphere. Secondly, ammonia was added as nitrogen source and by way of hydrothermal treatment, ammonia would uniformly diffuse from the surface to the bulk of TiO_2 sphere. Lastly, after calcination at 400 °C, the template CTAB was removed, producing worm-like pores. Nitrogen atom was introduced into the lattice of crystalline TiO_2 nanocrystals which are assembled to a sphere. The substitution N atoms are highly dispersed into the bulk of n-N-TiO_2 sphere to achieve the homogeneous doping of N from the bulk to the surface of TiO_2 sphere, which is expected to improve the visible light photocatalytic activity.

The morphologies of p-TiO_2, m-TiO_2 and N doped TiO_2 spheres are characterized by HRTEM and the images are presented in Fig. 1. It can be seen from images (Fig. 1a, d and g) that the as-prepared multiple TiO_2 nanoparticles are spherical with smooth surface and a relatively uniform diameter in the range of 400–600 nm. The spheres get avoided aggregations and were uniformly distributed as PVP was added as dispersant. The amplified images of the sphere edge (Fig. 1b, e and h) reveal that the prepared TiO_2 sphere is composed of large amounts of small TiO_2 nanocrystals with the size of about 10–13 nm. Compared with Fig. 1b of solid p-TiO_2 consisted of close packed nanocrystals, Fig. 1e and h displays the worm-like structure of undoped and N doped mesoporous TiO_2 spheres, which has a striking contrast with the void-free p-TiO_2, suggesting that the addition of CTAB has the tendency to produce aggregated pores and increases the specific surface area. In Fig. 1c, f and i, the lattice spacing of all the samples is ~0.35 nm, ascribed to the (1 0 1) plane of the anatase phase. In addition, from the macro-prospective (SEM images shown in Fig. 2), we can also see that p-TiO_2, m-TiO_2 and N doped TiO_2 are all spherical. All these characteristics indicate that the process of nitrogen doping did not affect the morphology and crystalline form of TiO_2 spheres.

The X-ray diffraction (XRD) pattern in Fig. 3a shows the phases of 0-N-TiO_2 and m-TiO_2 formed at the same calcination temperature. The peaks of m-TiO_2 are low-intensity and ambiguous, but its crystallinity improved distinctly after the hydrothermal process. During the hydrothermal treatment, the ammonia diffused into the bulk and the surface of TiO_2 spheres. After the calcination, N was doped into the surface and subsurface lattice of TiO_2 nanocrystals. It could contribute to strengthen the polymorph. Additionally, the phases of TiO_2 spheres with different content of nitrogen doping are shown in Fig. 3b. The crystallinity of N doped TiO_2 sphere is better than that of 0-N-TiO_2, demonstrating that N doping facilitates the crystallinity. The average crystal size and d-spacing of different samples determined by XRD using Scherrer equation are shown in Table 1. We can also figure out that the crystallite particles which consist of TiO_2 spheres are estimated to be 12 nm in size. As shown in the figure, compared with the amorphous phase of m-TiO_2, the characteristic diffraction peaks at 25.4°, 37.9°, 48.0°, 54.1°, 63.0° are observed for all n-N-TiO_2 samples, presenting good agreement with the anatase phase (JCPDS card No. 21-1272). Besides, there are no other peaks such as Ti-N and N-O detected in the samples, which may be ascribed to the reason that the content of N was too little to be tested. It can be concluded from XRD patterns that N doping is conductive to improve the crystallinity, thus to promote the photocatalytic activity. Besides, the "d" space values of all the samples remain unchanged, indicating that doping modification does not change the average unit cell dimension. In addition to that, with the increase of the nitrogen, the size of TiO_2 has an obvious decrease due to the lattice distortion induced by the N doping (Table 1), which is in accordance with our previous work [9].

Furthermore, in order to further testify the crystalline phase and investigate the effect of N doping on the structure of TiO_2 spheres, the Raman spectroscopy was carried out and the images are shown in Fig. 4. There are five main peaks for each sample, that is, the Raman line at 145 cm^{-1}, 197 cm^{-1}, 398 cm^{-1}, 516 cm^{-1} and 639 cm^{-1}, which can be assigned to E_g, E_g, B_{1g}, $A_{1g}+B_{1g}$ and E_g modes of the anatase phase, respectively [24,25]. Moreover, there are no other characteristic peaks detected from the images which stand for other phases. This result is consistent with the XRD result.

The surface area and porosity of these TiO_2 spheres were investigated via nitrogen adsorption–desorption isotherms shown in Fig. 5. Fig. 5b and c shows the classic type IV-like isotherm with H_2 hysteresis loops, indicating that both m-TiO_2 and nitrogen doped TiO_2 spheres have uniform mesopores. Conversely, Fig. 5a reveals the inexistence of mesoporous material in p-TiO_2 due to the absence of CTAB. The Barrett–Joyner–Halenda (BJH) pore sizes, determined from the adsorption branches (the inset of Fig. 5), and Brunauer–Emmett–Teller (BET) surface areas are shown in Table 1. By comparison of the surface area of p-TiO_2 (24.9 m^2/g) and m-TiO_2 (83.1 m^2/g), it can be concluded that the addition of CTAB

Table 1
Parameters of m-TiO_2 and N doped mesoporous TiO_2 sphere with different amount of nitrogen doping.

Sample	Crystallite size (nm)	*d* spacing (Å)	Surface area (m^2/g)	Pore size (nm)
p-TiO_2	25.7	3.5	24.9	–
m-TiO_2	13.4	3.5	83.1	7.2
0-N-TiO_2	13.9	3.5	84.8	8.8
0.2-N-TiO_2	12.1	3.5	94.9	7.8
0.5-N-TiO_2	11.4	3.5	139.6	7.0
0.8-N-TiO_2	12.3	3.5	129.0	9.3
1.0-N-TiO_2	11.2	3.5	122.0	9.1
2.0-N-TiO_2	11.9	3.5	127.0	9.2

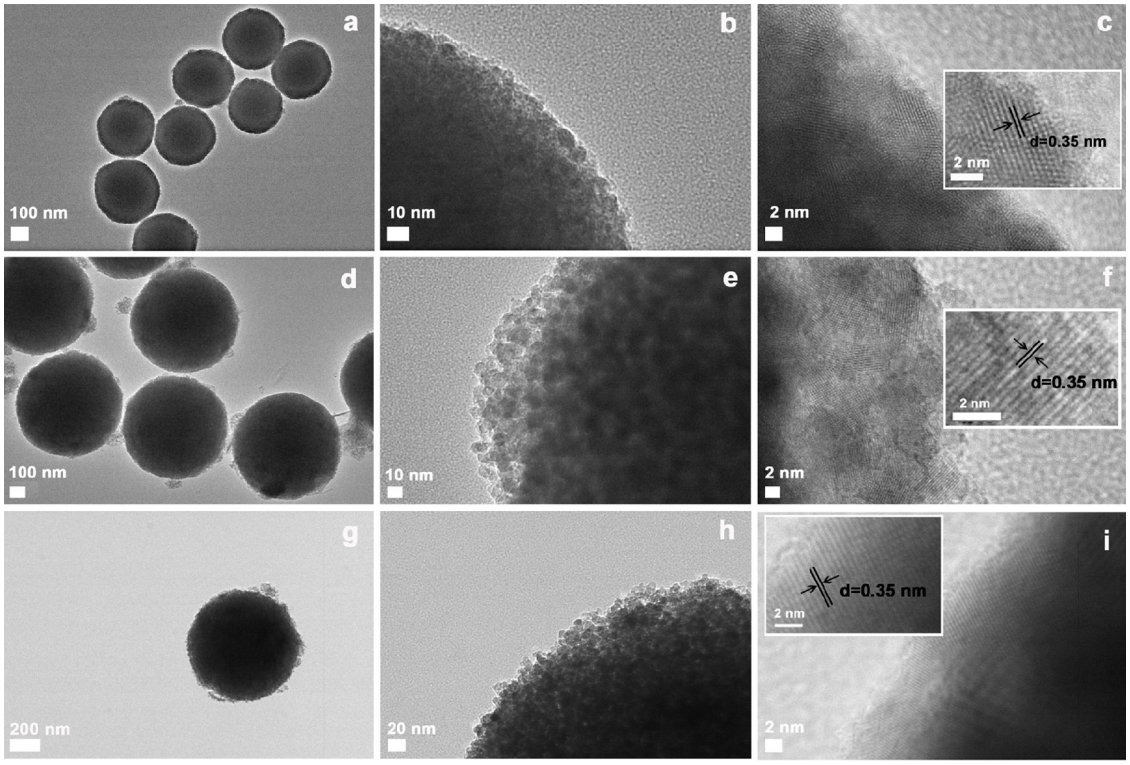

Fig. 1. HRTEM images of p-TiO_2 (a–c), m-TiO_2 (d–f) and N doped mesoporous TiO_2 spheres (g–i).

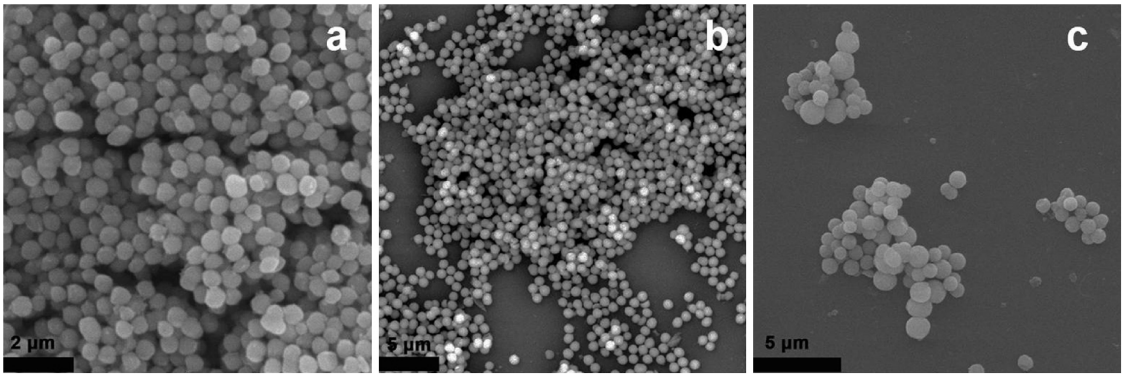

Fig. 2. SEM images of p-TiO_2 (a), m-TiO_2 (b) and N doped mesoporousTiO_2 spheres (c).

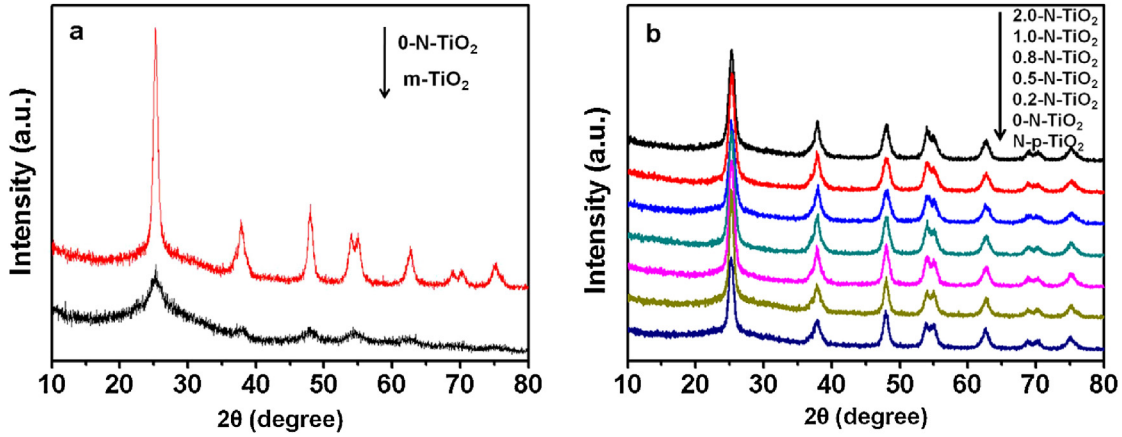

Fig. 3. XRD patterns of (a) 0-N-TiO_2 and m-TiO_2, (b) n-N-TiO_2 and N-p-TiO_2 samples with different amount of nitrogen doping.

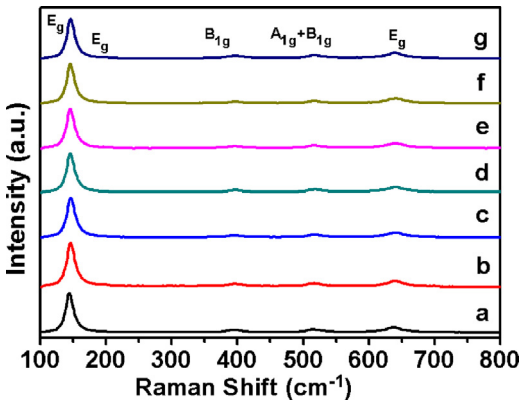

Fig. 4. Raman spectra of (a) 0-N-TiO_2, (b) 0.2-N-TiO_2, (c) 0.5-N-TiO_2, (d) 0.8-N-TiO_2, (e) 1.0-N-TiO_2, (f) 2.0-N-TiO_2, (g) N-p-TiO_2.

conduced to increase the specific area and pore-forming after calcination. With the nitrogen doping modification, the surface area increased to a large extent (shown in Table 1). However, the average pore size changed from 7.0 nm to 9.3 nm, probably resulting from the partial sintering of mesoporous structure. Among them, note that 0.5-N-TiO_2 has the relatively lower pore size (7.0 nm) and higher specific area (139.6 m^2/g). It is very interesting that the nitrogen doping can increase the pore size and surface area of TiO_2 at the same time. It is worth mentioned that the nitrogen doping causes a wide pore size distribution and the pore size in the range of 2–5 nm has a significant increase (Fig. 5c), which is responsible for the increase of surface area. With the doping of nitrogen into the lattice of TiO_2, the decreased size of TiO_2 nanocrystals can increase the aggregated pore size in the range of 2–5 nm, and the lattice distortion induced by the N doping can increase the surface charge to enhance the repulsive force between nanoparticles, resulting in the change of average pore size from 7.0 nm to 9.3 nm. A relatively high specific area of nitrogen doped TiO_2 spheres could facilitate the diffusion of reactant molecules and offer more active sites for adsorption, resulting in the photocatalytic process more efficient.

The UV–visible diffuse reflectance spectra show the light absorption properties of mesoporous TiO_2 spheres with different amount of N doping, shown in Fig. 6. For comparison, the spectrum of undoped mesoporous TiO_2 sphere is also illustrated. The band gap absorption edge of 0-N-TiO_2 sample is approximately 400 nm and does not exhibit noticeable absorption in the visible region. However, interestingly, all of the N doped TiO_2 catalysts display distinct and meaningful absorption covering the whole visible region of 400–800 nm. Therefore, we can conclude that the degree of N doping could influence the visible light absorption of mesoporous TiO_2 spheres. Nevertheless, instead of reducing the recombination of photoelectrons and holes, too much N can result in the formation of photoelectron recombination centers.

To detect the chemical compositions and elemental environments of N-dopant, the as-synthesized N doped mesoporous TiO_2 spheres were analyzed by XPS. The results show that N doped TiO_2 contains Ti, O, N and C elements. The C element can be ascribed to the adventitious carbon contaminants or residual organic carbons from the XPS instrument. Fig. 7 shows the N 1s XPS spectra of N doped mesoporous TiO_2 spheres with different amount of N doping. It can be seen that there is a broad peak between 399 and 403 eV in all N doped catalysts, which is characteristic of N doping, and three peaks are discovered by fitting the curves. We attribute the peak at 399.5 eV (peak 1) to substitutional N for O in the form of O–Ti–N bonding [26], 400.6 eV (peak 2) to the surface adsorption of N_2 [27] and 401.5 eV (peak 3) to nitrogen species bound

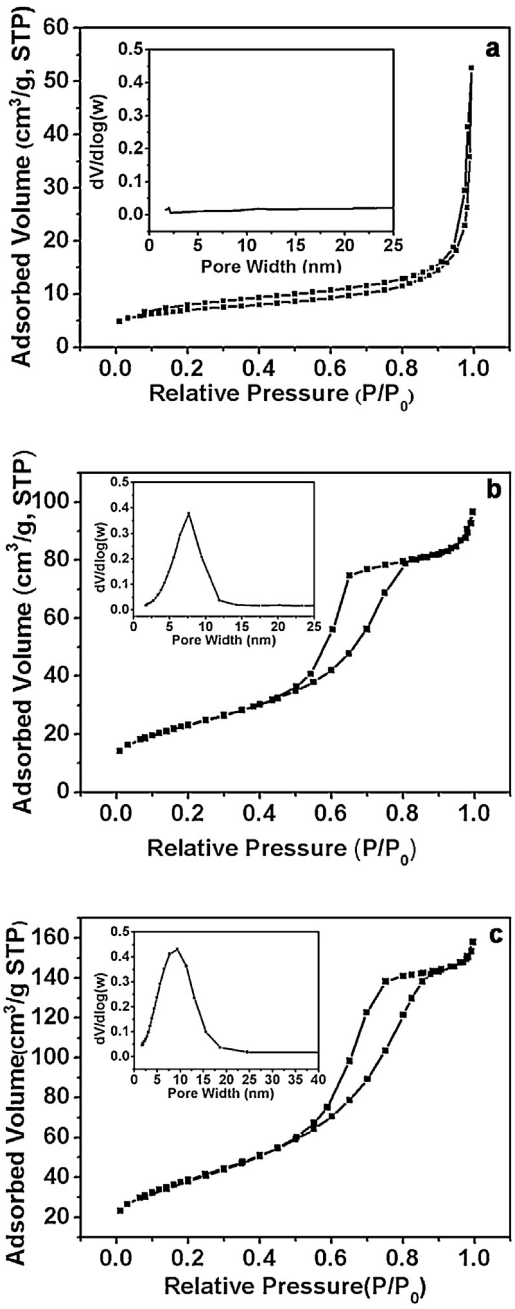

Fig. 5. Nitrogen adsorption–desorption isotherm and pore size distribution (the inset) of (a) p-TiO_2, (b) m-TiO_2 and (c) 0.5-N-TiO_2.

to various surface oxygen sites (such as adsorbed NO_x) [9,28–30]. TiO_2 doped with N could absorb the visible light, which is also testified by degradation of RhB mentioned in the following process. Asahi et al. [27] have made a point that nitrogen doped into substitutional sites of TiO_2 is indispensable for band-gap narrowing and photocatalytic activity improving. As shown in Fig. 7, the intensities of peak 1 in different samples are inconsistent and such differences caused the discrepancy of their photocatalytic activities.

Compared with the nitrogen doped in the solid TiO_2 sphere, the nitrogen concentration in the mesoporous TiO_2 sphere is much higher, which increases from 0.17% to 1.31% (Fig. 8). In the preparation process, the CTAB is filled in the interstice of TiO_2 nanocrystals, which makes the stacked nanocrystals become fluffy (Scheme 1). The loose packing structure is in favor of the further filling of

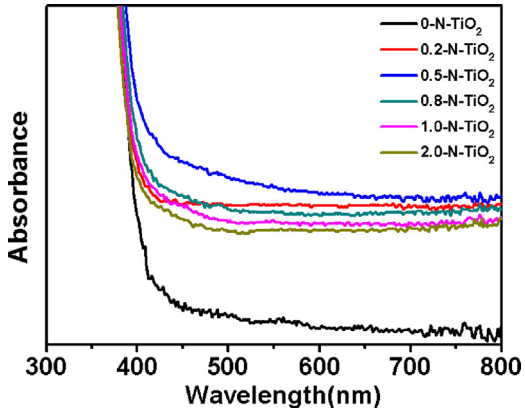

Fig. 6. UV–visible diffuse reflectance spectra of undoped and N doped TiO_2 spheres with different amount of N doping.

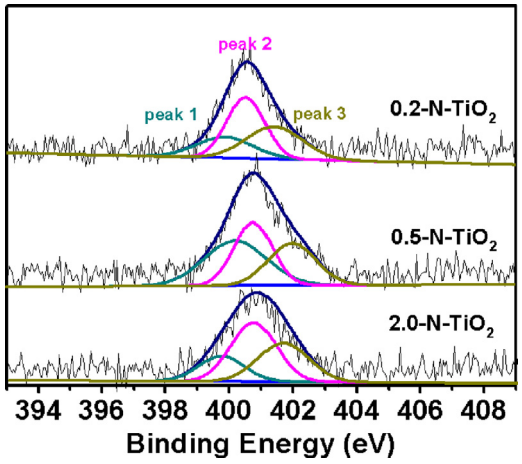

Fig. 7. XPS spectra of 0.2-N-TiO_2, 0.5-N-TiO_2 and 2.0-N-TiO_2 at the N 1s region.

ammonia in the interstice of TiO_2 nanocrystals. Every TiO_2 nanocrystal is surrounded with ammonia molecules, and the nitrogen is introduced into every TiO_2 nanocrystal lattice by the hydrothermal and calcination treatment. To every TiO_2 nanocrystal, the nitrogen doping is heterogeneous, but to the whole mesoporous TiO_2 sphere, the nitrogen doping is homogeneous. A mass of heterogeneous N doped TiO_2 nanocrystals assemble into a homogeneous N doped TiO_2 sphere. Compared with the solid

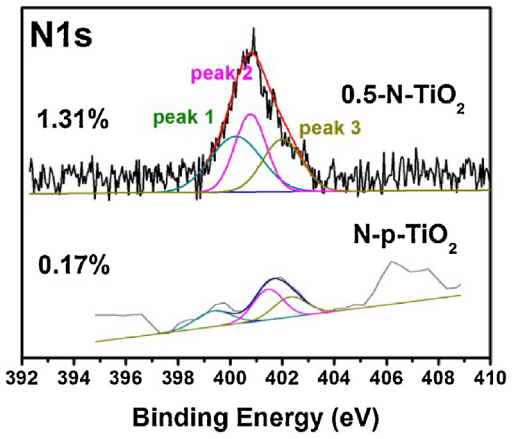

Fig. 8. XPS spectra of 0.5-N-TiO_2 and N-p-TiO_2 at the N 1s region (the peak intensity of N-p-TiO_2 is amplified to be convenient for the comparison).

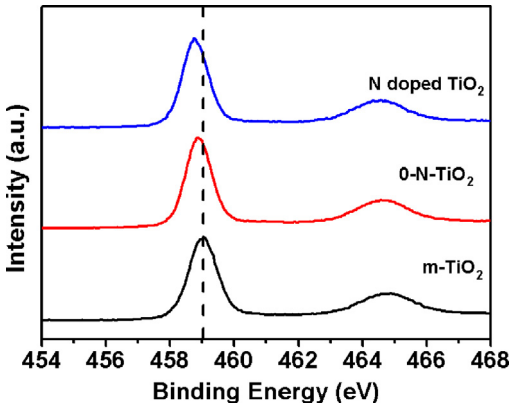

Fig. 9. XPS spectra for Ti 2p region of m-TiO_2, 0-N-TiO_2, and N doped mesoporous TiO_2 sphere.

TiO_2 sphere (N-p-TiO_2), the contact between TiO_2 nanocrystals and ammonia in 0.5-N-TiO_2 is significantly increased, resulting in an enhanced doping concentration.

Moreover, the presence of small amount of surface Ti^{3+} is verified from the Ti 2p XPS spectra shown in Fig. 9. The spin-orbit split lines of Ti $2p_{3/2}$ and Ti $2p_{1/2}$, characteristics of Ti (IV) oxidation state, can be observed at around 459 eV and 465 eV, respectively. The binding energy of Ti $2p_{3/2}$ peak of N doped TiO_2 spheres shifts to the low field after the hydrothermal process and nitrogen doping. This phenomenon is ascribed to the substitution of a less electronegative nitrogen atom in the place of oxygen atom, increasing the electron density around Ti [25], thus facilitating to produce some surface Ti^{3+}. It is worth mentioned that only when the nitrogen doping concentration is high enough to destroy the charge balance of TiO_2 sphere, some surface Ti^{3+} can be generated to recover a charge balance. The presence of Ti^{3+} further demonstrates the high substitution of N in the mesoporous TiO_2 sphere.

The photocatalytic degradation of RhB under visible light irradiation was carried out to evaluate the photocatalytic activities of N doped mesoporous TiO_2 spheres and specify the effect of the doping concentration. The results are presented in Fig. 10. Fig. 10a shows the adsorption ability of all samples. Specific area plays an important role in the adsorption effect. The photocatalysts with relatively high specific area could provide more active sites to the diffusion of reactant molecules and adsorption, resulting in the photocatalytic process more efficient. It can be seen that via nitrogen doping, the degradation rate of solid or mesoporous TiO_2 spheres was improved by comparison with the undoped sample (Fig. 10b). As is known to all, there are such factors which could have an influence on the photocatalytic activity as surface area, particle size, crystallinity or band gap values of photocatalysts [31]. The increase in the photocatalytic activity can be ascribed to the nitrogen doping effect which results in the response to the visible light more efficient. As mentioned above, among all the prepared undoped and N doped mesoporous TiO_2 spheres, the 0.5-N-TiO_2 sample has certain unique properties such as relatively high specific area (139.6 m^2/g, Table 1), relatively little particle size (7.0 nm, Table 1), pure anatase phase, high doping concentration and high UV–vis absorption capacity, which improve the access of RhB to inside and outer surfaces and provide abundant active sites. Compared with the nitrogen doped solid TiO_2 sphere, the 0.5-N-TiO_2 has larger surface area and higher N doping concentration, which determine the much better activity. Therefore, it demonstrates the best photocatalytic activity to decompose RhB under the visible light irradiation. That is, we consider the optimal nitrogen doping value as 0.5.

The photocatalytic mechanisms are explained as followings. TiO_2 nanocrystals were close stacked together to form the solid

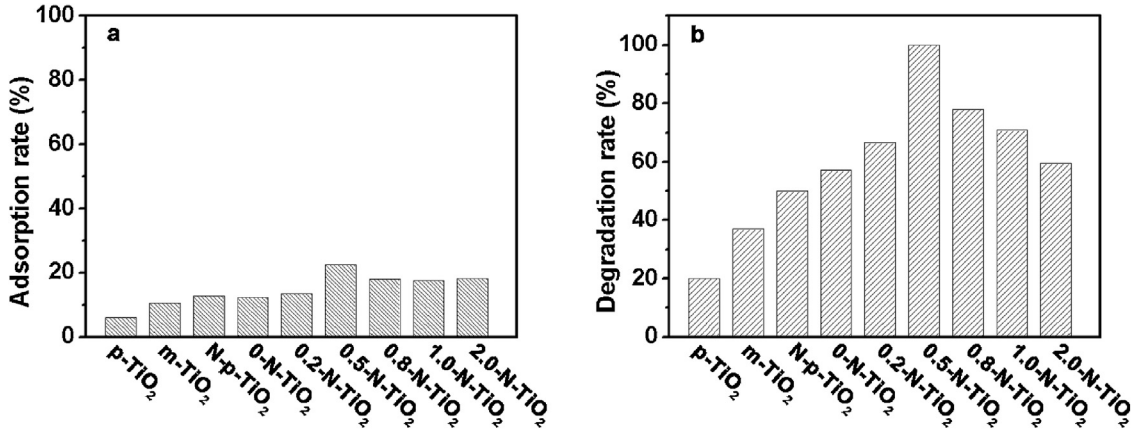

Fig. 10. Adsorption rate (a) and photocatalytic degradation rate (b) of RhB of undoped and N doped TiO_2 spheres under the visible light irradiation.

TiO_2 sphere, and after the doping of nitrogen, some impurity levels are distributed on the surface of subsurface of TiO_2 sphere, as shown in Scheme 2a. The close packing structure of solid TiO_2 sphere determines the difficulty of nitrogen doping in the bulk of spheres. Different from that, the loose packing of TiO_2 nanocrystals in the presence of CTAB induces a mesoporous structure, which was conductive for TiO_2 spheres to suck up ammonia into interspaces (Scheme 1). Compared with undoped TiO_2 spheres, the doping concentration of N doped TiO_2 sphere was uniformly distributed from the inside out, producing the successive energy bands from the bulk to the surface (Scheme 2b). These N doping introduced successive impurity energy levels are located above the valance band and cut down the band gap of TiO_2 sphere, inducing a wide visible-light response in the range of 400–800 nm. In view of that, the special packing approach of TiO_2 nanocrystals in the presence of PVP and CTAB gives a mesoporous sphere structure, which provides the possibility of homogeneous doping of nitrogen in the bulk of TiO_2 sphere. To the whole of TiO_2 sphere, the homogeneous doping achieves the generation of successive impurity levels distributed from the bulk to the surface, which is responsible for the extension of photocatalytic activity to the whole visible-light range of 400–800 nm.

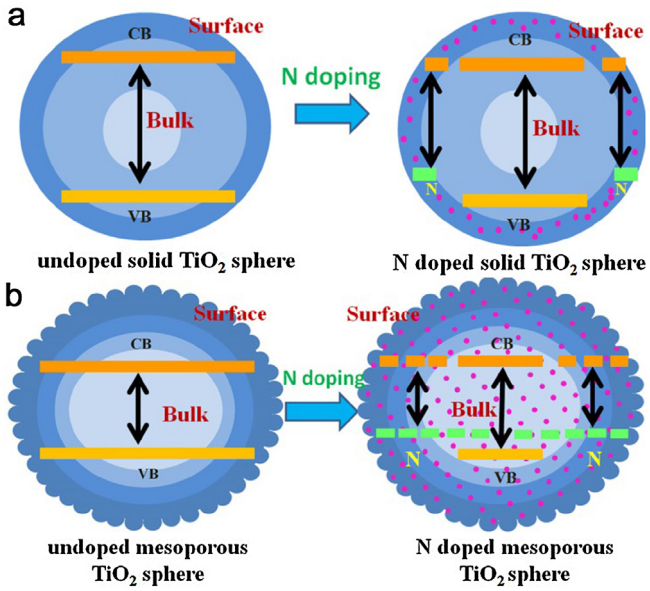

Scheme 2. Schematic diagrams of band structures of undoped and N doped solid (a) and mesoporous (b) TiO_2 spheres.

4. Conclusions

In summary, a series of N doped mesoporous TiO_2 spheres consisted of nanosized crystals were successfully synthesized. The nitrogen doping was uniformly distributed from the surface to the bulk and induced the successive impurity levels inside the band gap of TiO_2 sphere. The nitrogen doped mesoporous TiO_2 spheres exhibit such excellent characteristics as high specific area, relatively small particle size, pure anatase phase, high N doping concentration and excellent UV–vis absorption capacity in the range of 400–800 nm, which are all beneficial to the photodegradation of Rhodamine B under the visible light irradiation. The photocatalytic activity was strongly influenced by the amount of N source added. Among all, the optimal one is 0.5-N-TiO_2. The generation of the successive impurity levels in the bulk of TiO_2 sphere plays an important role in the high photocatalytic activity.

Acknowledgements

This work has been supported by the National Nature Science Foundation of China (21173077, 21377038, 21203062 and 21237003); the National Basic Research Program of China (973 Program, 2013CB632403), Science and Technology Commission of Shanghai Municipality (12230705000, 12XD1402200); the Research Fund for the Doctoral Program of Higher Education (20120074130001) and the Fundamental Research Funds for the Central Universities.

References

[1] A.L. Linsebigler, G. Lu, J.T. Yates Jr., Chem. Rev. 95 (1995) 735–758.
[2] M.R. Hoffmann, S.T. Martin, W. Choi, D.W. Bahnemann, Chem. Rev. 95 (1995) 69–96.
[3] K. Xu, Y. Guo, Q. Sun, S. Dong, Z. Li, Res. Chem. Intermediat. 39 (2013) 1417–1428.
[4] Y. Cong, B. Tian, J. Zhang, Appl. Catal. B: Environ. 101 (2011) 376–381.
[5] M. Xing, Y. Wu, J. Zhang, F. Chen, Nanoscale 2 (2010) 1233–1239.
[6] M. Xing, D. Qi, J. Zhang, F. Chen, B. Tian, S. Bagwas, M. Anpo, J. Catal. 294 (2012) 37–46.
[7] X. Wu, S. Yin, Q. Dong, C. Guo, H. Li, T. Kimura, T. Sato, Appl. Catal. B: Environ. 142–143 (2013) 450–457.
[8] B. Qiu, M. Xing, J. Zhang, J. Am. Chem. Soc. 136 (2014) 5852–5855.
[9] Y. Cong, J. Zhang, F. Chen, M. Anpo, J. Phys. Chem. C 111 (2007) 6976–6982.
[10] S. Yuan, Q. Sheng, J. Zhang, H. Yamashita, D. He, Micropor. Mesopor. Mater. 110 (2008) 501–507.
[11] H. Hao, J. Zhang, Mater. Lett. 63 (2009) 106–108.
[12] H. Zhou, D. Li, M. Hibino, I. Honma, Angew. Chem. Int. Ed. 44 (2005) 797–802.
[13] T. Shu, P. Xiang, Z.-M. Zhou, H. Wang, G.-H. Liu, H.-W. Han, Y.-D. Zhao, Electrochim. Acta 68 (2012) 166–171.
[14] H.J. Nam, T. Amemiya, M. Murabayashi, K. Itoh, Res. Chem. Intermediat. 31 (2005) 365–370.
[15] Z. Jiang, F. Yang, N. Luo, B.T.T. Chu, D. Sun, H. Shi, T. Xiao, P.P. Edwards, Chem. Commun. (2008) 6372–6374.

[16] H.-J. Kim, J.-D. Jeon, S.-Y. Kwak, Powder Technol. 243 (2013) 130–138.
[17] J. Li, W. Wan, H. Zhou, J. Li, D. Xu, Chem. Commun. 47 (2011) 3439–3441.
[18] Q. Xiang, J. Yu, W. Wang, M. Jaroniec, Chem. Commun. 47 (2011) 6906–6908.
[19] H.-E. Wang, J. Jin, Y. Cai, J.-M. Xu, D.-S. Chen, X.-F. Zheng, Z. Deng, Y. Li, I. Bello, B.-L. Su, J. Colloid Interface Sci. 417 (2014) 144–151.
[20] L.-S. Zhong, J.-S. Hu, L.-J. Wan, W.-G. Song, Chem. Commun. (2008) 1184–1186.
[21] D. Grosso, G.J. de, A.A. Soler-Illia, E.L. Crepaldi, B. Charleux, C. Sanchez, Adv. Funct. Mater. 13 (2003) 37–42.
[22] Q. Wu, W. Li, D. Wang, S. Liu, Appl. Surf. Sci. 299 (2014) 35–40.
[23] H.-G. Jung, Y.S. Kang, Y.-K. Sun, Electrochim. Acta 55 (2010) 4637–4641.
[24] W. Zhang, Y. He, M. Zhang, Z. Yin, Q. Chen, J. Phys. D: Appl. Phys. 33 (2000) 912.
[25] S.-H. Liu, H.-R. Syu, Appl. Energy 100 (2012) 148–154.
[26] W. Wei, L. Chunhua, S. Mingxing, N. Yaru, X. Zhongzi, Chin. J. Catal. 33 (2012) 629–636.
[27] R. Asahi, T. Morikawa, T. Ohwaki, K. Aoki, Y. Taga, Science 293 (2001) 269–271.
[28] Y. Ao, J. Xu, S. Zhang, D. Fu, Appl. Surf. Sci. 256 (2010) 2754–2758.
[29] X. Chen, X. Wang, Y. Hou, J. Huang, L. Wu, X. Fu, J. Catal. 255 (2008) 59–67.
[30] Z. Hu, L. Xu, J. Chen, Mater. Lett. 106 (2013) 421–424.
[31] Y. Takahara, J.N. Kondo, T. Takata, D. Lu, K. Domen, Chem. Mater. 13 (2001) 1194–1199.